Hindawi Publishing Corporation
Journal of Nanomaterials
Volume 2012, Article ID 350425, 11 pages
doi:10.1155/2012/350425

Research Article

Micromechanism and Kinetic Formulation of Vertically Aligned ZnO Nanorods Grown on Catalytic Bilayers

Dong-Hau Kuo and Jheng-Yu He

Department of Materials Science and Engineering, National Taiwan University of Science and Technology, Taipei 10607, Taiwan

Correspondence should be addressed to Dong-Hau Kuo, dhkuo@mail.ntust.edu.tw

Received 17 May 2012; Accepted 26 July 2012

Academic Editor: Renzhi Ma

Vertically aligned ZnO nanorods were grown at 700°C for 2 h on sapphire substrates with catalysts in bilayer configurations of Sn (top)/Ni (bottom) and Sn/In, where the top layer is formed by sputtering and the bottom one is deposited by spin coating. The effects of bilayer catalysts on growth kinetics of nucleation and growth, growth micromechanism, and vertical alignment of growing ZnO nanorods have been investigated. The vertical alignment of the Sn/Ni-catalyzing ZnO nanorods is determined at the initial nucleation stage, where the nuclei are formed as regular candlestick-like platforms. The reason for the formation of the candlestick-like nuclei is due to the contribution of strain energy built in the underlying catalyst bilayers. The variations of axial and radial dimensions with growth duration for the growth of ZnO rods were explained and data fitting with the aids of kinetic growth equations, which are based upon the well-known ledge model for crystal growth from vapor and diffusion kinetics.

1. Introduction

Zinc oxide (ZnO) is a direct bandgap semiconductor with a wide bandgap of 3.37 eV and large exciton binding energy (60 meV). This semiconductor has been attractive for optoelectronic applications in light-emitting diodes and laser diodes at room temperature. Nanometer scale, one-dimensional (1D) materials, such as nanowires, nanorods, and nanotubes, have become of great interest due to their potential applications in nanolaser, field emission devices, photovoltaic, piezoelectric transducers, photocatalysts, chemical, and biosensors, and so forth.

The vapor-phase growth of 1D ZnO has been widely conducted with Zn and (ZnO + graphite) powders as reactants. The most uniform and vertically aligned (VA) ZnO nanorods with a diameter of 50–150 nm have been grown by using the carbothermal reaction above 850°C on Au catalyst-patterned sapphire substrates with the aids of submicrometer sized polystyrene balls [1] and laser-hardening lithography technology [2, 3] or by using the Zn source at 750°C on sapphire substrates covered with a *c* axis-oriented ZnO buffer layer [4]. Because no droplets on the tips of flat-ended nanorods have been observed, the self-catalytic growth mechanism or the vapor-solid mechanism is used to explain the growth behaviors. However, the self-catalytic mechanism needs to consider the oxidation of catalysts during the growth period. The vapor-liquid-solid growth mechanism has been applied for nanowires with dome-shaped droplets on its tips. The formation of catalyst droplets and its durability through the growth process without oxidation or nitridation are the major concerns.

Gold has been the most important and reliable catalyst for growing 1D ZnO, because it has demonstrated the capability to grow uniform and aligned nanorods. The preference of Au catalyst is related to its high-temperature stability in oxidizing atmosphere. Other catalysts such as Ni, Sn, Cu, have also been examined, but their uniformity and size in diameter need to be improved. ZnO rods grown by thermal evaporation on the Ni-coated silicon had a large size of 300–350 nm in diameter [5]. By using Sn catalyst, a liquid Sn droplet was located on the tip of ZnO nanorods to assist the orientation-aligned growth [6, 7]. Catalyst has been recognized as a requisite to perform the 1D catalyst-confined growth. In order to understand the growth micromechanisms, we ever used Au-containing bilayer catalysts of Au/Al, Au/Ni, and Au/In to grow randomly oriented

ZnO rods on silicon wafer substrates with diameters of ~100, 400, and 800 nm, respectively [8]. To make a further progress in order to grow well-aligned ZnO nanorods instead of micrometer sized and randomly oriented ZnO rods on the bilayer catalyst-covered substrates without using Au as a catalyst, we had investigated different unilayer or bilayer configurations made by mixed-solution coating, sputtering, polymer dispersant in coating solution, substrate etching techniques [9–11]. The one with the promising result is the ZnO rods grown on the Fe-covered [9] and Sn/Ni bilayer substrates [11]. We have continued efforts on the growth of ZnO nanorods by using the bilayer configurations. There were few works to grow ZnO nanorods with a bilayer catalyst. With our variations in the bilayer configurations, we demonstrate in this paper with different growth modes and different micromechanisms.

From our systematic works, I have a better control in growing the well-aligned ZnO rods. *Without the better growth control, the measurements of rod dimensions in repeated experiments with different growth durations will be very difficult and not reliable, which is the reason for the difficulty and limited reports in kinetic study*. After we can provide reliable and controllable techniques to grow the uniform and vertically aligned ZnO nanorods with a size of ~110 nm in diameter by utilizing the bilayer catalysts of Sn/Ni and Sn/In, we intend to investigate the ZnO nanorods grown at different growth periods to explore the growth kinetics and the relations among the bilayer catalysts, the initial nucleation stage, and the subsequent growth stage. Kinetic growth equations are derived, which are based upon the variations of the axial and radial dimensions with the growth duration, and they are fitted well to our growth data. Some of works had measured the length/diameter changes with growth period, but only the interpretations were mentioned without rate equations to explain and fit their growth data individually in the axial and radial directions.

2. Experimental

ZnO nanowires were grown at 700°C for 2 h on the catalyst-coated Si wafer or sapphire substrates by thermal evaporation under a mixture flow of 10-sccm (standard cubic centimeter per minute) O_2 and 200-sccm N_2 with a Zn mixture of Zn and ZnO at a weight ratio of 1.0 g : 1.0 g or 1 : 1. The Zn mixture together with substrate was loaded on a graphite support. The preparation of catalyst layers involved spin coating and direct current (d.c.) sputtering. A similar experimental approach is listed in [9]. The spin coatings of Sn, In, and Ni catalysts involved the 0.01 M solutions of tin chloride, indium nitrate, and nickel nitrate, respectively, followed by pyrolysis at 650°C for 30 min and reduction at 850°C for 30 min in an (Ar + 7% H_2) mixed gas. Each pyrolyzed oxide had a film thickness of ~0.1 μm. For d.c. sputtering, Sn, In, and Ni films were deposited at output powers of 20 and 70 watts for 1 min for coating Sn and Ni, respectively, and of 5 watts for 3.5 min for depositing indium. These metallic catalyst layers had a thickness of 30–60 nm for each. In addition to the single-layered catalysts, bilayer catalysts of Sn/Ni and Sn/In were also prepared. The bilayer catalysts were constituted by spin coating a bottom layer followed by sputtering a top layer. The symbol of Sn/Ni, as an example, represented a Sn-sputtered coating on top of a Ni-spin coated layer. After spin coating and pyrolysis of the Ni layer, the reduction reaction was executed after the Sn layer was sputtered on the nickel oxide. The sapphire substrates for the Sn/Ni system were etched by a 0.1 M NaOH solution. The substrate for the Sn/In system was not etched. The etching did not change the vertical alignment but was beneficial for obtaining slender 1D ZnO. To study the growth kinetics, ZnO nanorods were grown at 700°C for different durations of 1 min, 5 min, 30 min, and 120 min on Sn/Ni and Sn/In sapphire substrate. Before heating, the growth chamber was pumped down by mechanical pump. During the heating stage, the system was under argon and the Zn vapor generated as temperature approached 700°C. When the temperature reached 700°C, the mixed (O_2 + N_2) gas flowed into this system. Therefore, the oxide growth started at the O_2-added stage. Scanning electron microscopes (SEM, JEOL JSM 6500F, Japan; Cambridge S360, UK) were used to observe the growth morphology. A field-emission scanning electron microscope (FESEM, JEOL JSM 6500F, Japan) was used to observe the growth morphology and to measure the rod dimensions in length and diameter. Phase identification, composition analysis, and microstructural characterization of nanowires were conducted by a transmission electron microscope (TEM, JEOL 3010, Japan) equipped with energy dispersive spectroscopy (EDS). Room-temperature photoluminescence (PL) measurements were performed using a 325 nm He-Cd laser as the excitation source.

3. Results

3.1. ZnO Growth on Catalytic Unilayers. Figure 1 shows SEM images of one-dimensional ZnO grown at 700°C for 2 h on (a), (b) Sn, (c), (d) In, and (e), (f) Ni (a), (c), (e) sputter or (b), (d), (f) spin coated silicon wafer substrates by thermal evaporation with a Zn mixture of Zn and ZnO in a weight ratio of 1.0 g : 1.0 g. The Sn-catalyzing 1D ZnO was in the form of nanowires with smaller diameters of 100 nm (Figure 1(a)) and 200 nm (Figure 1(b)). The In-catalyzing growth contained nonuniform ZnO crystals including rods of 200–300 nm in size and larger leaf-like crystals (Figures 1(c) and 1(d)). The Ni-catalyzing 1D ZnO grown on Si wafer substrates were in the form of inclined and hexagonal-shaped rods with a larger diameter of 800 nm–1.5 μm for those spin coated (Figure 1(f)) and in the form of leafs with a large dimension in 600 nm–1.2 μm for those sputtered (Figure 1(e)). There is no difference for ZnO from the Sn catalyst, which can be attributed to its melt state at different catalyst size. However, the difference in the ZnO shape from the Ni catalyst can be related to the catalyst size, which in the solid state has led to different crystallinities. Catalysts of Sn, In, Ni spin coated with nitrate or chloride solutions can be reduced to form metallic droplets for Sn and Ni but it remains as an oxide layer for In catalysts. No matters of metallic indium or indium oxide, the grown ZnO had no

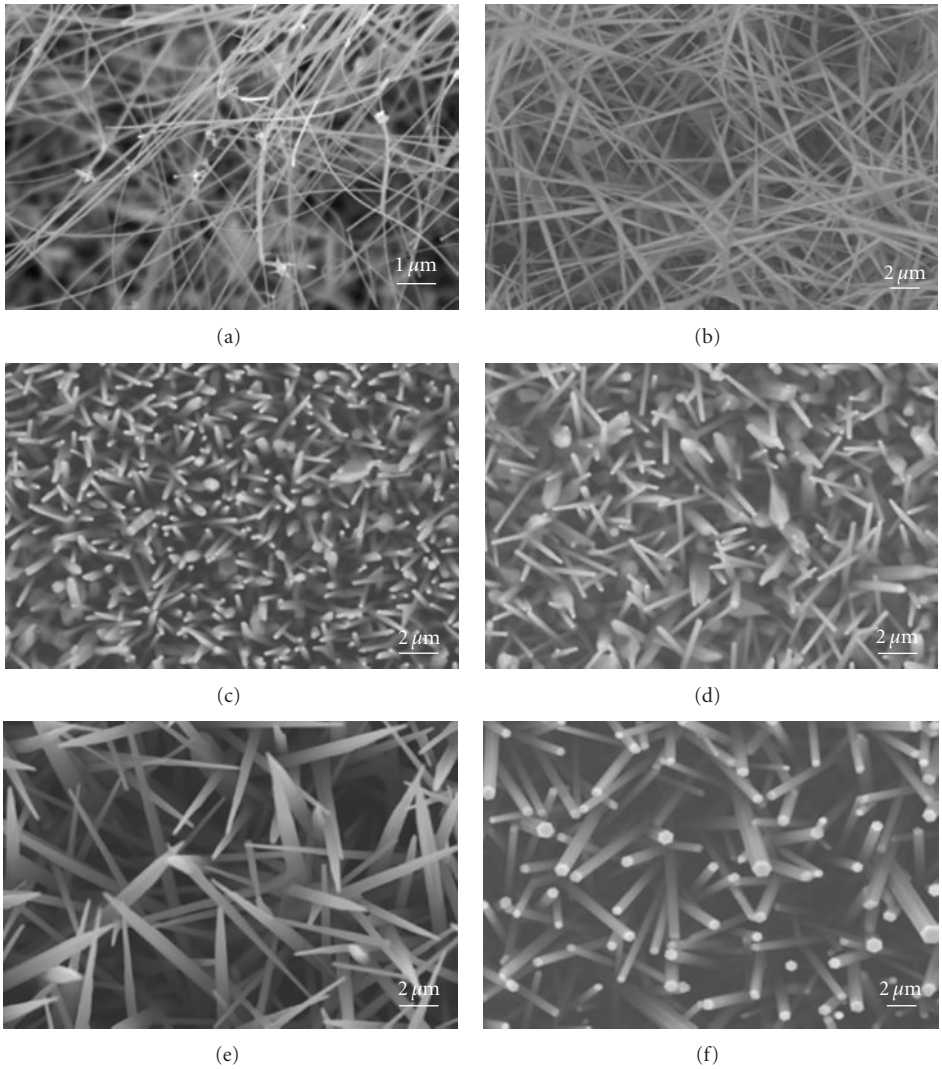

Figure 1: SEM images of one-dimensional ZnO grown at 700°C for 2 h on (a), (b) Sn, (c), (d) In, and (e), (f) Ni (a), (c), (e) sputter- or (b), (d), (f) spin coated silicon wafer substrates by thermal evaporation with a Zn mixture of Zn and ZnO in a weight ratio of 1.0 g : 1.0 g.

big differences for the sputtered and the spin coated ones. From these experiments, the Sn catalyst generates the finest nanowires and the spin coated Ni catalyst favors to form ZnO nanorods with a hexagonal cross-section. However, the size of these hexagonal-shaped ZnO was in a sub-micrometer scale. 1D ZnO rods grown with the Ni catalyst have constantly suffered the problem of large diameters [5].

3.2. ZnO Growth on Catalytic Bilayers. Two types of bilayer catalysts used to assist the 1D ZnO growth include Sn/Ni and Sn/In. Figure 2 displays surface morphologies of ZnO nanorods grown at 700°C for (b) 1 min, (c) 5 min, (d) 30 min, and (e) 120 min on Sn sputter/Ni spin coated sapphire substrates. After growing for 1 min, no 1D formed and only nuclei were observed. ZnO nanorod arrays with a hexagonal cross-section had formed with a length of 0.4 ± 0.1 μm and a diameter of 100 ± 20 nm in 5 min from pyramid platforms, which behaved like a candle rod sits on a candlestick. These pyramid platforms were examined at higher magnifications, as can be seen in the inset of Figure 2(c). With increasing growth time, nanorods increase apparently on its length but not on its diameter. After a 2-h growth duration, the grown ZnO rods had a length of 30 ± 10 μm and a diameter of 110 ± 25 nm. The image of as-fabricated Sn/Ni bilayer catalyst, after pyrolysis at 650°C for 30 min and reduction at 850°C in an Ar-5% H_2 mixture gas for 30 min, is shown in Figure 2(a). Before the ZnO growth, the Sn/Ni bilayer catalyst had become spheroidal. After the 1-min growth, the spheroidal catalysts disappear and the substrates were covered with the oxidized Zn-covering layers. The 2D growth on 1D-ZnO had been observed by metal-organic chemical vapor deposition [12].

Figure 2(f) shows the PL spectra of the VA-ZnO nanorods shown in Figure 2(e). From the PL spectra, it can be seen that the vertically aligned ZnO nanorods only show a sharp and strong peak at approximately 383.3 nm (3.24 eV), which corresponds to the near-band-edge peak that is

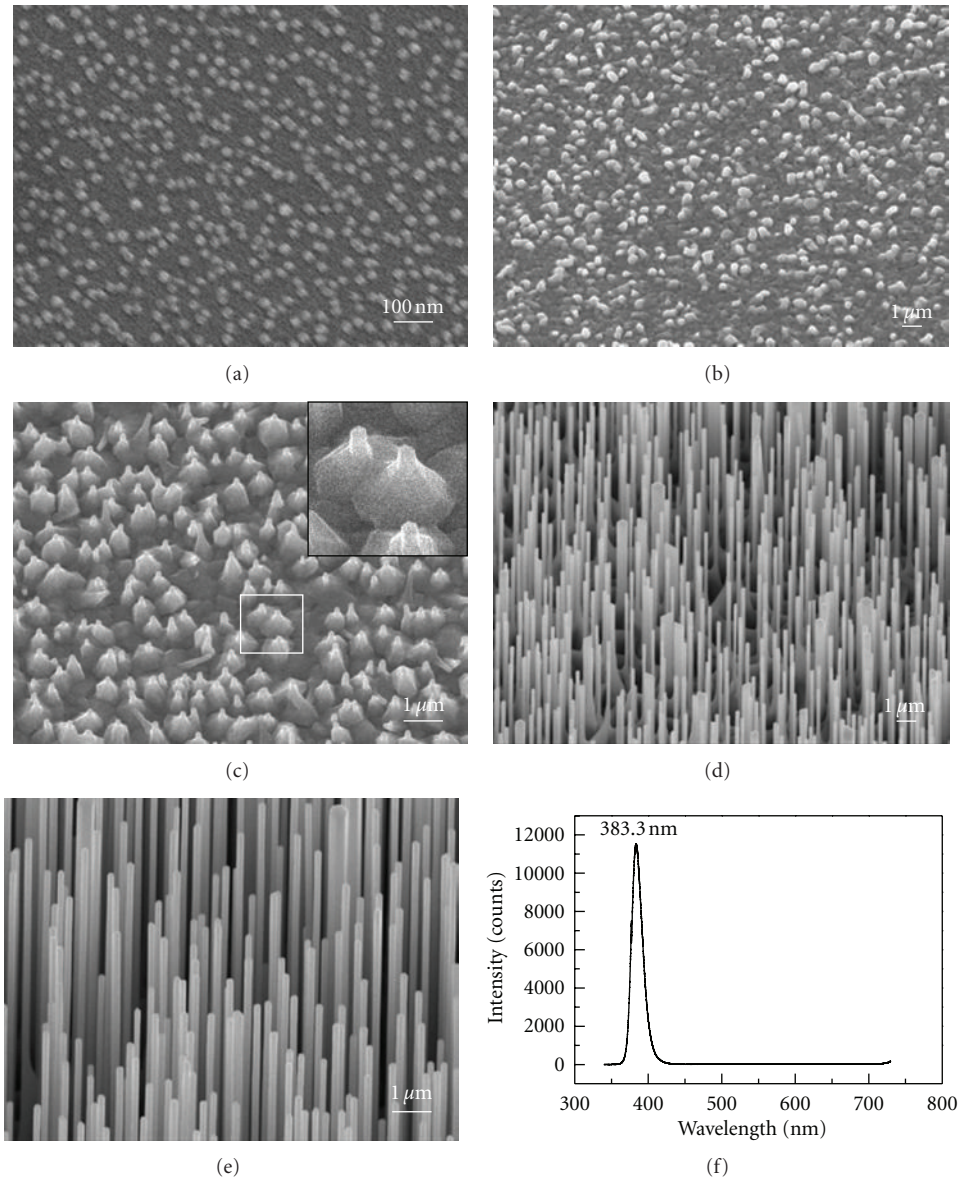

Figure 2: Surface morphologies of ZnO nanorods grown at 700°C for (b) 1 min, (c) 5 min, (d) 30 min, and (e) 120 min on Sn sputter-/Ni spin coated sapphire substrates by thermal evaporation with a Zn mixture of Zn and ZnO in a weight ratio of 1 : 1. (a) SEM image of Sn sputter-/Ni spin coated bilayer catalysts after pyrolysis at 650°C for 30 min and reduction at 850°C in a Ar-5% H_2 mixture gas for 30 min. (f) Photoluminescence spectra for the vertically aligned ZnO nanorods in (e). The substrates were etched by a 0.1 M NaOH solution for 15 s. The inset in (c) was enlarged from the white square-selected area.

responsible for the recombination of free excitons through an exciton-exciton collision process [13–15]. A full width at half maxima value of 145 meV for this excitonic emission was obtained [16]. The appearance of a sharp and strong near-band-edge emission in the UV region without any deep level emission in the visible region indicates that the as-grown ZnO nanorods showed good crystallinity with a good optical property and few structural defects such as oxygen vacancies and interstitials of zinc. Therefore, based upon the bilayer catalyst-assisting growth, VA-ZnO nanorods with a good ultraviolet emission quality can be grown from pyramidal platforms or nuclei with parallel (0001) planes to the substrate surface.

Figure 3 displays surface morphologies of ZnO nanorods grown at 700°C for (b) 1 min, (c) 5 min, (d) 30 min, and (e) 120 min on Sn/In bilayer-coated sapphire substrates. The Sn/In catalysts remained as a layer on substrates (Figure 3(a)). The sputtered Sn layer inhibited by the underlying In_2O_3 layer did not become spheroidal after 850°C annealing. ZnO nuclei formed after the 1-min growth duration (Figure 3(b)). The ZnO nanorods directly grown from the catalytic buffer layer had a length of $0.75 \pm 0.25\,\mu$m and a diameter of 250 ± 30 nm in 5 min without the platform nuclei available (Figure 3(c)). With the increase in the growth duration, the length and diameter of nanorods apparently increased. After a 2-h growth duration, the grown ZnO

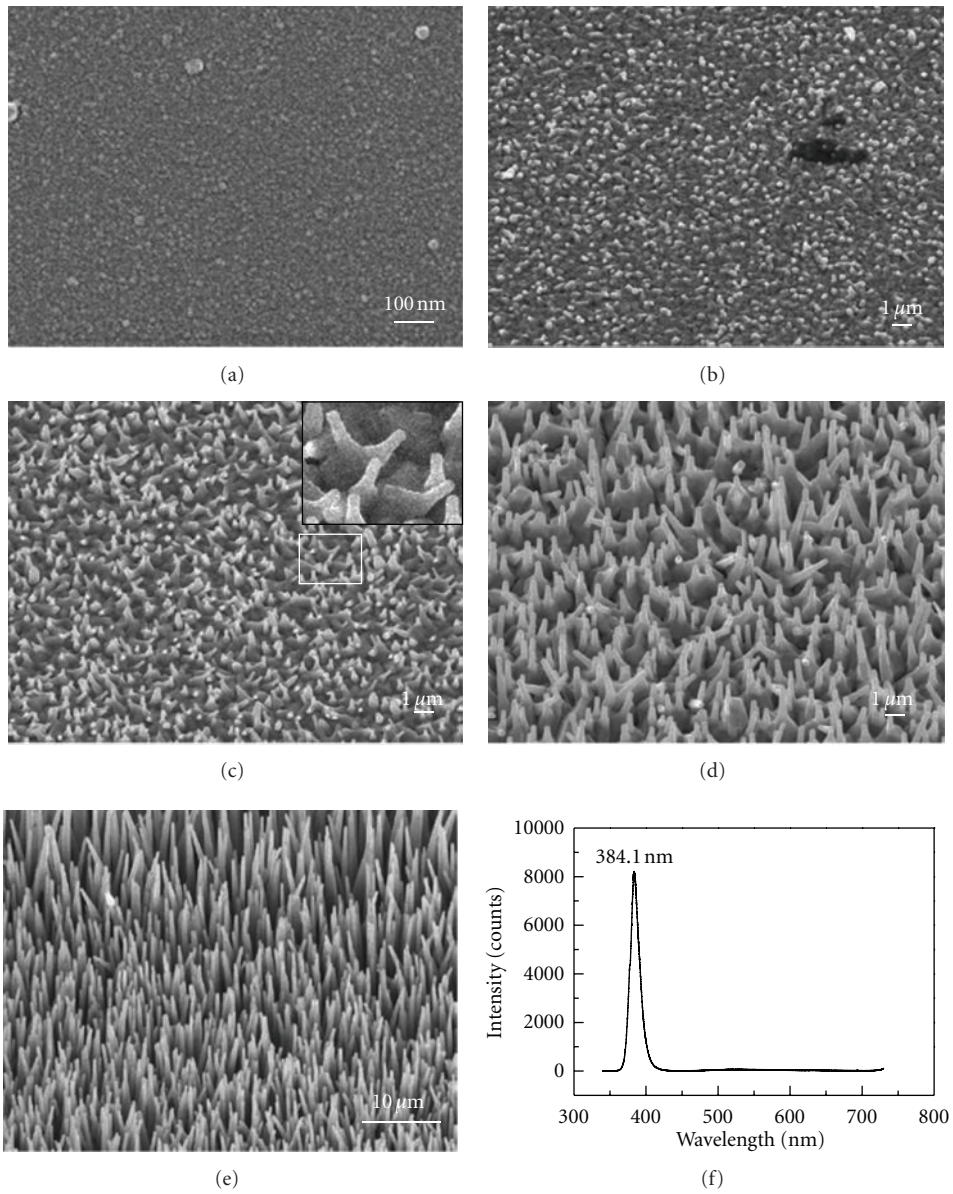

Figure 3: Surface morphologies of ZnO nanorods grown at 700°C for (b) 1 min, (c) 5 min, (d) 30 min, and (e) 120 min on Sn sputter-/In spin coated sapphire substrates by thermal evaporation with a Zn mixture of Zn and ZnO in a weight ratio of 1 : 1. (a) SEM image of Sn sputter-/In spin coated bilayer catalysts after pyrolysis at 650°C for 30 min and reduction at 850°C in an Ar-5% H_2 mixture gas for 30 min. (f) Photoluminescence spectra for the vertically aligned ZnO nanorods in (e). The inset in (c) was enlarged from the white square-selected area.

rods had a length of 25 ± 5 μm and a diameter of 400 ± 55 nm (Figure 3(e)). Although the Sn/In-catalyzing ZnO rods had a hexagonal shape in cross-section, but these rods were not aligned. The inset in Figure 3(c) shows an enlarged image to observe the initial growth stage of ZnO nanorods. There were no larger, well-defined, and isolated pyramid platforms spreading on the ZnO-covering substrate surface. Figure 3(f) shows the PL spectra of the VA0-ZnO nanorods shown in Figure 3(e). The aligned ZnO nanorods display a sharp and strong peak at approximately 384.1 nm (3.23 eV). This nanorod showed a similar result in photoluminescence measurement as that shown for ZnO obtained from the Sn/Ni catalyst (Figure 2(f)). The similar performance indicates the different catalyst configurations only change the growth behaviors but do not introduce growth defects.

3.3. Dimensional Changes in the Axial and Radial Directions. The growth kinetic study of 1D ZnO is executed by measuring the changes of the axial and radial dimensions with the growth duration. Figures 4(a) and 4(b) show the variations of the diameter and length of ZnO nanorods grown at 700°C for different durations of 1, 5, 30, 120 min on (a) Sn/Ni- and (b) Sn/In-coated sapphire substrates. Both of the systems

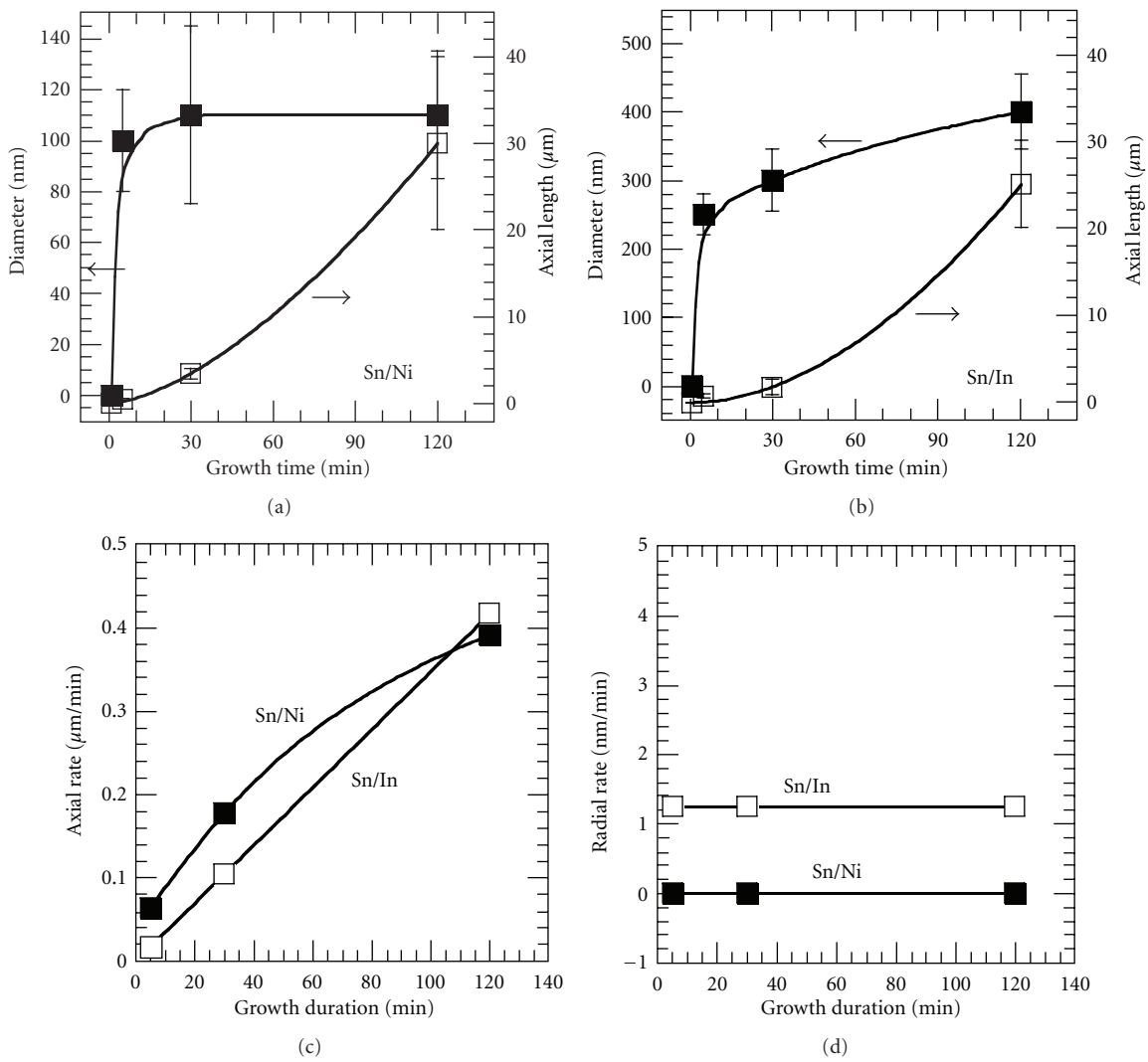

Figure 4: Growth behaviors in terms of the diameter and length of ZnO nanorods grown at 700°C for different durations of 1, 5, 30, 120 min on (a) Sn/Ni- and (b) Sn/In-coated sapphire substrates by a thermal evaporation-oxidation method with a Zn mixture of Zn and ZnO in a weight ratio of 1 : 1. The variations of axial and radial rates, obtained by curve fitting the 5-, 30, and 120-min data followed by retrieving from the derivatives of the best-fitting equations, with growth duration are shown in (c) and (d), respectively.

display a slight different trend. The Sn/Ni-catalyzing rods after growing for 5 min and 2 h have diameters of 100 ± 20 and 110 ± 25 nm, respectively, and lengths of 0.4 ± 0.1 and 30 ± 10 um. The stage for the first few minutes belongs to nucleation. The growth stage began apparent after a 5-minute growth period. The axial and radial growth rates can be derived at different periods, excluding the nucleation stage, as shown in Figures 4(c) and 4(d), by curve fitting the wire length-growth duration plot, followed by retrieving from the derivatives of the curve-fitting equations to obtain growth rates at the durations of 5, 30, and 120 min. *This approach needs to be emphasized, because the growth rate is not obtained from the measured length divided by our growth duration. The conventional approach is related to an average growth rate during a growth period, but our approach is to obtain an instantaneous rate.* For the Sn/Ni system, the lengthening rate was proportional to the time exponent of 1/2 and the thickening rate is zero. The lengthening and thickening rates were proportional to the time exponents of 1 and 0 for the Sn/In system.

4. Discussion

4.1. ZnO Growth. From the previous experimental data, two comparable systems of Sn/Ni and Sn/In have been obtained. The Sn/Ni system has grown the vertically aligned ZnO nanorods from the regularly aligned candlestick-like nuclei. The growth of ZnO rods from this system is a nucleus-confined growth. It only grows in the axial direction. The Sn/In system has grown the incompletely aligned rods from the ZnO-covering buffer layer. It does not show the apparent nuclei, as the candlestick-like nuclei do. These rods grow in both the axial and radial directions. By using the apparently

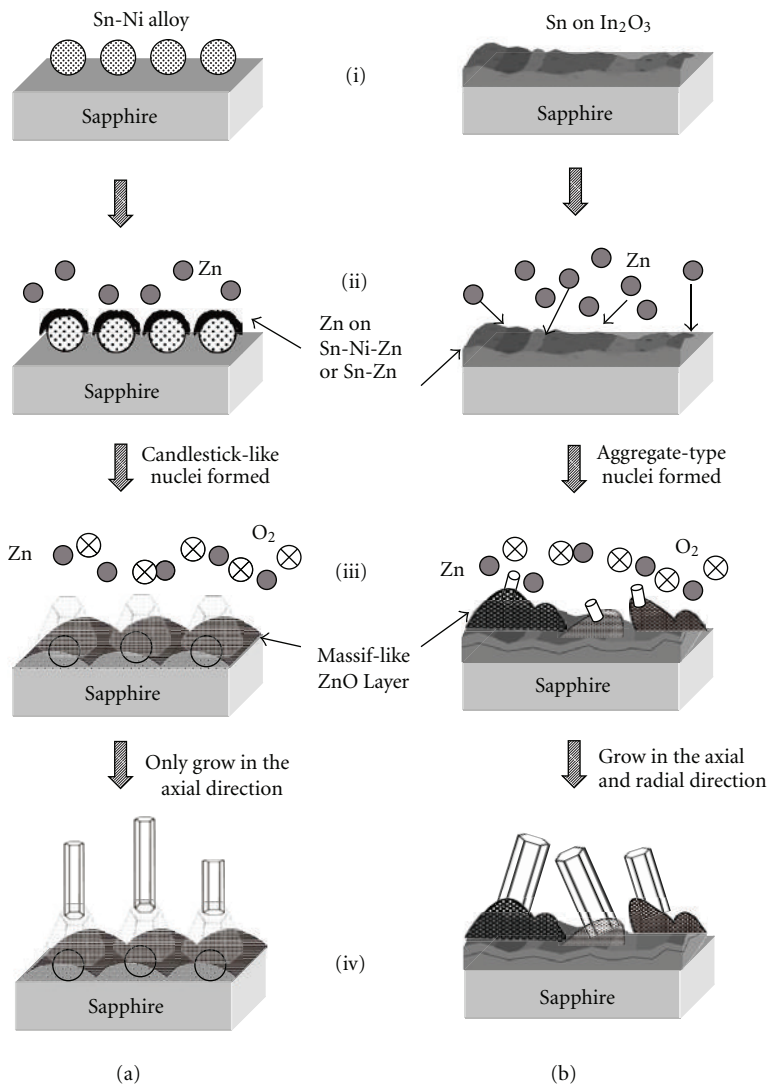

Figure 5: Schematic growth micromechanisms for (a) vertically aligned ZnO nanorod array grown on the Sn sputter/Ni spin coated sapphire substrates and for (b) slightly slant ZnO nanorods grown on the Sn/In coated substrates.

different systems for comparative purposes, the reasons for the growth behavior and dimensional change need to be explained and embodied by a formulated equation.

4.2. Our Proposed Growth Micromechanisms. From the observations of Figures 2 and 3, it is observed that the style of nuclei formed at the early stage of nucleation determines the vertical alignment of 1D ZnO. Figure 5 shows the schematic diagrams of the growth micromechanisms of the bilayer-catalyzing ZnO nanorods with the (a) vertically aligned and (b) slightly slant modes. The nuclei can be easily distinguished in the Sn/Ni system, where the flat-end pyramid-shaped islands form as candlestick-like platforms to provide the sites for growing ZnO nanorods with a hexagonal cross-section. On the other hand, the Sn/In system does not show the well-defined nuclei or the candlestick-like platforms and has grown slightly slant ZnO nanorods directly from the large-grained ZnO buffer layer by aggregating the adsorbed adatoms through a short-range diffusion to form the nuclei. Briefly speaking, the Sn/Ni system has the platforms on the massif-like ZnO-covering layer but the Sn/In system only has the ZnO rods grown from the massif-like layer. The different nucleation behaviors can lead to the different inclination in alignment. The obvious reason for the differences of these two systems is related to the different components of nickel in the Sn/Ni system and indium in the Sn/In system. For the as-fabricated catalyst images in Figures 2(a) and 3(a), isolated catalyst droplets have formed in the Sn/Ni system, but it is not the case for the Sn/In system (Figure 5(i)). The nonreducible In_2O_3 films inhibit the spheroidization of metallic Sn in the Sn/In system (Figure 5(b-i)). Before oxygen enters the reactor at 700°C, zinc vapor liberates during the heating cycle. The vaporized Zn will condense and cover on substrates (Figure 5(ii)), react with the spheroidal catalysts (Figure 5(a-ii)), and be oxidized once oxygen is introduced (Figure 5(a-iii)) [17]. For the Sn/Ni system, the

ZnO buffer layers embedded inside with reacted spheroidal catalysts are composed of large grains and favor to nucleate flat-end or (0001) plane-oriented pyramid platforms. The flat ends of those platforms orient parallel to the (0001) plane-oriented sapphire substrates in order to establish the well-aligned nanorods. After a 1-minute growth period (Figure 2(b)), the nuclei or platforms are not obvious. After a 5-minute growth period, the pyramidal nuclei have formed with protruded nanorods of 0.4 μm in length. It can be induced that the nucleation step is accomplished within the first five minutes. After a 2-h growth duration, our nucleus platforms behave as candlesticks regularly sitting on the massif-like table ready for growing VA-ZnO nanorods with a diameter of ~110 nm.

For the Sn/In system, the ZnO buffer layers underlying with flat Sn/In_2O_3 catalyst layers (Figures 5(b-ii) and 3(b)). Nucleation occurs randomly and does not form the flat-end pyramid platforms. Once the nuclei grow to a critical size, the ZnO nanorods are directly grown from the massif-like ZnO layers in an inclined orientation via the reactant adsorption from vapor, surface diffusion of adatoms, zinc-oxygen reactions, and the desorption for the surplus reactants (Figure 5(b-iii)). As the ZnO growth continues, the rods increase its dimensions in length and diameter (Figure 5(b-iv)). However, the formation of isolated catalyst droplets cannot guarantee the vertical alignment of ZnO nanorods. To have regularly aligned ZnO nanorods, the formation of the candlestick-like platforms is the critical factor. Therefore, the choice of the catalyst combination is very important, which can lead to different catalyst properties, reactions, and stress states. Based on the nucleation and growth theory for crystal growth, the extra built-in strain energy in the Sn/Ni system assists nucleation by overcoming the formation energy of pyramidal nuclei. There is no sufficient built-in strain energy for the Sn/In system due to the softness of Sn metal in the form of flat layer. Growth mechanisms of randomly oriented 1D ZnO with nanopen-, nanonail-, or nanopencil-like structure on pyramids have been proposed in literatures, however, their pyramids had a comparatively large dimension to form the pen-like shape [18, 19]. Kim et al. have been aware that the nanosheets with several facet planes play a significant role in the evolution of ultraslim and vertical ZnO nanowire arrays [20]. However, their nanosheets are similar to the previously proposed self-catalyzing ZnO buffer layers.

4.3. Kinetics and Kinetic Model. Our candlestick-like nuclei restrict the thickening of ZnO nanorods. When the axial dimensions of ZnO rods increase exponentially with the growth duration, their radial dimensions do not change for the Sn/Ni system but have a big change for the Sn/In system (Figure 4(b)). The irrelevance of our radial dimension in the Sn/Ni system with growth time is similar with the growth of carbon nanotubes (CNTs) and can be attributed to the nucleus-confined growth behavior. The reported diameters of 1D ZnO increased with growth time [21, 22]. Tsao et al. reported a linear relation. For the axial dimension, it increases fast but levels off at long durations for CNTs [23]. A linear relation between the length of nanowires and growth time for 1D ZnO has been reported [21, 24]. Reports with experimental growth data in the axial and radial directions simultaneously changed with growth duration are rare. The trends of rod length or diameter in the growth kinetics have been mentioned, but the explanations and data fitting with *kinetic equations* are much difficult. What the relevance is between the changes of rod length and diameter needs more understanding, regardless to say the data fitting for the rod length and diameter together with kinetic equations. However, we will use kinetic equations to fit and explain the growth rates in radial and axial directions together. The systematical dimension measurements at different durations for kinetic understanding are our major approach to probe the growth kinetic problems. This work is totally different from our previous work on the developments of aligned and well-controlled ZnO rods, but they provide the basis for our progress in kinetics [8–11].

To analytically formulate the vapor-solid growth rates, the kinetic of the well-known ledge model (Figure 6(a)) and the surface diffusion (Figure 6(b)) needs to be considered [25, 26]. *Although this mechanism has been well developed, there are no reported data referring or fitting to the equations derived from such a ledge mechanism*. The reactants from vapors will gas-phase diffuse through a boundary layer to surface and become adatoms. The adatoms will propagate on surface through surface diffusion to execute reactions and find stable sites to reside. There are two directions on the step ledge, one is for ledge lengthening and the other is for thickening (Figure 6(a)). Li et al. proposed the growth mechanisms of tapered ZnO nanowire arrays with the aids of step velocity and radial growth rate [27]. They mentioned only the concept of the ledge velocity and radial velocity for the tapering angle. Shi et al. proposed the lattice step ledges as preferred places for nucleation of ZnO by the oxidation of Zn on step ledges [28]. Both of them did not present the experimental data in growth rates. Based upon the conservation of mass transporting from the vapor and migrating on the surface, the ledge velocity for a multiple-growth step condition is formulated as [25]

$$\begin{aligned} v_{\text{ledge}} &= \frac{\sqrt{2}(C_\infty - C_e)\lambda}{N^* \cdot \tau} \times \tanh\left(\frac{d}{\sqrt{2}\lambda}\right) \\ &= \frac{\sqrt{2}(S-1)Z_e\lambda}{N^*} \times \tanh\left(\frac{d}{\sqrt{2}\lambda}\right), \end{aligned} \tag{1}$$

where C_∞ is the concentration of reactants in the gas phase far away from the growing interface, C_e the equilibrium concentration at vapor-solid interface, C_i the interface concentration, C_p the concentration of ZnO crystal, d the distance between steps, Z_e the stream of colliding reactants per unit time in equilibrium on interfaces, λ the mean diffusion distance between adsorption and evaporation, N^* the number of sites per unit area on crystal surface, τ the mean time of stay for adatoms, S the supersaturation (C_∞/C_e), and C_e defined as $Z_e \cdot \tau$. In the ledge mechanism, the adsorbed reactant vapor will evaporate if it resides far away from steps. Although this equation is derived from a

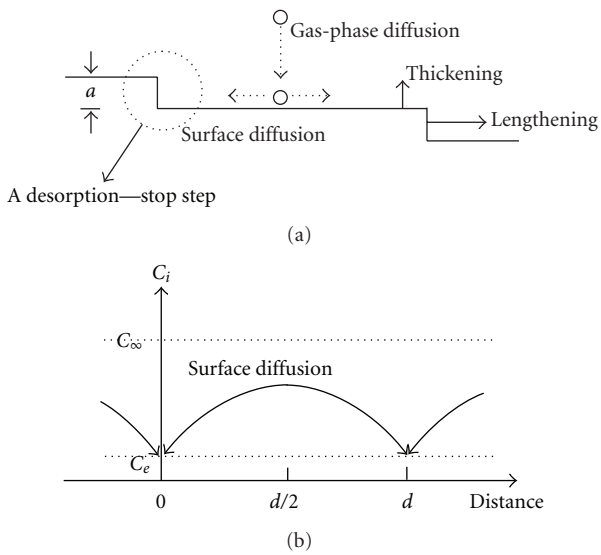

Figure 6: (a) Schematic configuration of the vapor-phase growth of ZnO rods *via* the combination of the ledge mechanism and diffusion processes, which involves the surface diffusion-controlled mechanism nearby the growing steps and the gas phase diffusion-controlled mechanism nearby the solid-vapor interface. The concentration profile for the surface diffusion-controlled growth mechanism is shown in (b).

well-known model, its utilization together with the growth data of one-dimensional crystals is rare.

Based upon the two-dimensional nucleation, d is proportional to the critical size of nuclei and inversely proportional to the formation energy of the nanorods (ΔG_f). ΔG_f related to the free energies of the gas-phase state and the equilibrium solid state is proportional to the $\mathrm{RT} \cdot \ln(C_\infty/C_e)$. Therefore, the step spacing can be related to supersaturation of $(S-1)$ as shown in (2) provided $(C_\infty - C_e) \ll C_e$ in a dilute gas phase [25]:

$$d \propto \frac{1}{\Delta G_f} = \frac{1}{\mathrm{RT} \cdot \ln(C_\infty/C_e)} \approx \frac{1}{\mathrm{RT} \cdot (C_\infty - C_e)/C_e} = \frac{1}{\mathrm{RT} \cdot (S-1)}. \quad (2)$$

Under a constant reactant flux, the apparent flux at the growth front of crystal gradually becomes increased because the crystal becomes longer. Therefore, one assumption is made here to have supersaturation $(S-1)$ proportional to $t^{1/2}$, that is, $(S-1) = k_1 t^{1/2}$ with k_1 a constant.

Our two systems with completely different behaviors in growth rates are discussed in the following sections with the viewpoint of kinetic formulation for the growth stage.

4.3.1. ZnO Nanorods Grown on Sn/Ni-Coated Substrates. These ZnO NRs grow faster at the axial direction but do not increase its dimension in diameter. The ZnO growth is confined by the candlestick-like nuclei to grow only in the axial direction (Figure 4(a)). It is assumed that the axial growth of smooth growing fronts of ZnO NRs is assisted by the "ledge mechanism." These ledges form on nuclei and on the flat-end top surface under a supersaturation growth condition in order to initiate the two-dimensional nucleation and growth processes. With the ledge growth mechanism, the lengthening rate can be expressed as

$$\frac{d\ell}{dt_{\mathrm{axial}}^{\mathrm{Sn/Ni}}} = \frac{a}{d} \times v_{\mathrm{ledge}}. \quad (3)$$

As higher strain energy is embedded in the Zn vapor-covering Sn/Ni layer, the ledges formed on the nuclei under supersaturation are a lot and their step spacing of d is quite smaller than the mean diffusion distance. With the condition of $d \ll \lambda$, (1) can be simplified as

$$\frac{d\ell}{dt_{\mathrm{axial}}^{\mathrm{Sn/Ni}}} \approx \frac{a}{d} \times \frac{\sqrt{2}(S-1)Z_e\lambda}{N^*} \times \left(\frac{d}{\sqrt{2}\lambda}\right) = \frac{a \cdot Z_e}{N^*}(S-1) \approx \frac{a \cdot Z_e}{N^*} \cdot k_1\sqrt{t}. \quad (4)$$

With this derivation, the axial rate of the Sn/Ni system is proportional to $t^{1/2}$, which is consistent with our experimental data in Figure 4(c).

As for a nil growth rate in diameter, it indicates the reactant vapor can only form nuclei on the flat-end cones. The nucleation on the smooth sides of hexagonal cones is difficult. The accommodation factor of reactant vapors for this system except on the flat-end top surface is almost negligible. The inability to build a radial rate can be related to the taller nuclei with steep edges, which is difficult to build the desorption-stop steps (Figure 6(a)) on nuclei. The desorption-stop step is the step in the ledge mechanism with the emphasis on its function to hold the adatoms. The adatoms without the desorption-stop steps cannot stick to that interface and will slip away or desorb from substrates.

Here, we need to clarify that the higher supersaturation due to larger strain energy can nucleate the growth steps with a short spacing (2). From the Sn/Ni system with a nil radial growth rate, we understand that supersaturation in vapor surrounding NRs is not helpful in building the heterogeneous nuclei on the NR sides. This behavior is also applied to the other system due to the same reactant flux. To differentiate these systems, the types of the desorption-stop steps on nuclei is important.

4.3.2. ZnO Nanorods Grown on Sn/In-Coated Substrates. These ZnO NRs have grown with a linearly increasing rate in the axial direction (Figure 4(c)) in addition to a constant thickening rate (Figure 4(d)). Our NR lengthening is analyzed with the similar equation of (1), but the condition becomes $d \gg \lambda$ and $\tanh(d/\sqrt{2} \cdot \lambda) \approx 1$. This hypothesis can

be supported by the smallest strain energy in the buffer layer. Therefore, (1) for the axial growth rate becomes

$$\begin{aligned}\frac{d\ell}{dt_{\text{axial}}^{\text{Sn/In}}} &\approx \frac{a}{d} \times \frac{\sqrt{2}(S-1)Z_e\lambda}{N*} \times 1 \\ &= k_2 a\text{RT}(S-1) \times \frac{\sqrt{2}(S-1)Z_e\lambda}{N*} \\ &= k_3(S-1)^2 \\ \frac{d\ell}{dt_{\text{axial}}^{\text{Sn/In}}} &\approx k_3\left(k_1 \cdot t^{1/2}\right)^2 = kt,\end{aligned} \tag{5}$$

where k, k_2, and k_3 are the proportional constants. With this derivation, the axial rate of the Sn/In system is proportional to t, which is consistent with the growth rate data in Figure 4(c).

Our NRs were thickened at the same time of the axial growth but with a slower rate. In order to increase the NR diameter, new absorbing adatoms need to arrive on the growing-stop steps of nuclei. Due to the smaller strain energy or the larger step distance, the attachment of reactant adatoms on the steps of nuclei is more difficult. In this situation, the ZnO growth on the desorption-stop steps of nuclei becomes a rate-determining factor, the NR thickening is controlled by the reactant reactions on the buffer layer-covering substrates, or the radial growth is an surface diffusion-controlled process (Figure 6(b)). For the interface-controlled growth, the growth rate or the thickening rate, proportional to the difference in chemical potentials ($\Delta\mu$) of reactions at interface and at equilibrium or approximately to the off-balance concentration ($C_i - C_e$) at moving interfaces (Figure 6(b)), can be expressed as

$$\begin{aligned}v_{\text{radial}}^{\text{Sn/In}} &= M \cdot (\text{force}) = M \cdot \frac{\Delta\mu}{V_m} \\ &= \frac{M\text{RT}}{V_m} \cdot \ln\left(\frac{C_i}{C_e}\right) \\ &\approx \frac{M\text{RT}}{V_m} \cdot \frac{C_i - C_e}{C_e},\end{aligned} \tag{6}$$

where M is the interface mobility, C_i is the concentration between steps, and V_m the molar volume of materials. Therefore, the thickening rate of the Sn/In system is almost constant, which is consistent with the experimental data in Figure 4(d).

Our proposed growth formulations are applied only for 1D ZnO grown by a vapor-solid mechanism. For the growth *via* a vapor-liquid-solid process, the diffusion in liquid droplets becomes the rate-determining step for lengthening as the wire diameter is determined by the catalyst size [29].

Growth behaviors of one-dimensional ZnO nanorods grown with a vapor-solid process are determined by the nucleus states of the buffer layer on substrates. With different surface modifications to generate different residual stress states in the buffer layers, the nucleation and growth behaviors for the rod growth become different, which reveal in the different growth behaviors in the axial and radial directions. With the successful equation formulations applied to different growth modes by using the basic kinetic model for crystals growing from vapor, the ZnO growth behaviors can be better elucidated and understood. Although some assumptions have been made and some considerations may not be complete, this work is trying to curve fit the experimental data with rate equations and to find the relevance between the axial and radial growth behaviors. In the Sn/Ni system, the ZnO growth occurs with the aid of the ledges on the flat-end top surface of the candlestick-like nuclei. No rod thickening is caused by the difficulty in the attachment of reactants on the side surface of camdlestick-like nuclei. For the Sn/In system, growths in the axial and radial directions simultaneously occur. Their lengthening provided by a ledge mechanism is determined by the step configuration. Their thickening is attributed to the attachment of reactant vapors to steps on nuclei through a surface diffusion-controlled process.

5. Conclusions

Vertically aligned ZnO nanorods were successfully grown on the bilayer catalyst-covered sapphire substrates with a length of 30 ± 10 μm and a diameter of 110 ± 25 nm by thermal evaporation at 700°C for 2h in the atmospheres of oxygen and nitrogen. The bilayer catalysts included Sn/Ni and Sn/In with the top and bottom layers prepared by sputtering and spin coating, respectively. Sn/Ni system shows a promising potential to grow vertically aligned ZnO nanorod arrays with a good ultraviolet emission from the regular and candlestick-like pyramid nuclei, which is aided by the strain energy built in the underlining catalyst layer. Without the pyramidal nuclei, slightly inclined nanorods in the Sn/In sytem were grown. The kinetic data of the growth rates in axial and radial directions for the Sn/Ni and Sn/In systems can be successfully curve fitted, correlated, and interpreted by kinetic equations, based upon the ledge mechanism for the vapor-solid crystal growth and diffusion kinetics.

Acknowledgment

The authors acknowledge the financial support by National Science Council under Grant No. 101-2221-E-011-046.

References

[1] H. J. Fan, B. Fuhrmann, R. Scholz et al., "Well-ordered ZnO nanowire arrays on GaN substrate fabricated via nanosphere lithography," *Journal of Crystal Growth*, vol. 287, no. 1, pp. 34–38, 2006.

[2] X. Wang, C. J. Summers, and Z. L. Wang, "Large-scale hexagonal-patterned growth of aligned ZnO nanorods for nano-optoelectronics and nanosensor arrays," *Nano Letters*, vol. 4, no. 3, pp. 423–426, 2004.

[3] D. S. Kim, R. Ji, H. J. Fan et al., "Laser-interference lithography tailored for highly symmetrically arranged ZnO nanowire arrays," *Small*, vol. 3, no. 1, pp. 76–80, 2007.

[4] L. Wang, X. Zhang, S. Zhao, G. Zhou, Y. Zhou, and J. Qi, "Synthesis of well-aligned ZnO nanowires by simple physical

vapor deposition on *c*-oriented ZnO thin films without catalysts or additives," *Applied Physics Letters*, vol. 86, no. 2, Article ID 024108, 3 pages, 2005.

[5] A. Umar, B. Karunagaran, E. K. Suh, and Y. B. Hahn, "Structural and optical properties of single-crystalline ZnO nanorods grown on silicon by thermal evaporation," *Nanotechnology*, vol. 17, no. 16, pp. 4072–4077, 2006.

[6] P. X. Gao, Y. Ding, and Z. L. Wang, "Crystallographic orientation-aligned ZnO nanorods grown by a tin catalyst," *Nano Letters*, vol. 3, no. 9, pp. 1315–1320, 2003.

[7] Y. Ding, P. X. Gao, and Z. L. Wang, "Catalyst-nanostructure interfacial lattice mismatch in determining the shape of VLS grown nanowires and nanobelts: a case of Sn/ZnO," *Journal of the American Chemical Society*, vol. 126, no. 7, pp. 2066–2072, 2004.

[8] D. H. Kuo and B. J. Chang, "From preannealing of bilayer catalysts to explore the growth micromechanisms of ZnO nanorods," *Crystal Growth and Design*, vol. 10, no. 2, pp. 977–982, 2010.

[9] D. H. Kuo, J. F. Fang, R. S. Chen, C. A. Chen, and Y. S. Huang, "ZnO nanomaterials grown with Fe-based catalysts," *Journal of Physical Chemistry C*, vol. 115, no. 25, pp. 12260–12268, 2011.

[10] D.-H. Kuo and B.-J. Chang, "Growth behaviors of ZnO nanorods grown with the Sn-based bilayer catalyst-covered substrates," *Journal of Nanomaterials*, vol. 2011, Article ID 603098, 9 pages, 2011.

[11] D.-H. Kuo, J.-Y. He, and Y.-S. Huang, "Synthesis of vertically aligned ZnO nanorods on Ni-based buffer layers using a thermal evaporation process," *Journal of Electronic Materials*, vol. 41, no. 3, pp. 451–456, 2012.

[12] S. H. Park, S. H. Kim, and S. W. Han, "Growth of homoepitaxial ZnO film on ZnO nanorods and light emitting diode applications," *Nanotechnology*, vol. 18, no. 5, Article ID 055608, 2007.

[13] S. C. Lyu, Y. Zhang, H. Ruh et al., "Low temperature growth and photoluminescence of well-aligned zinc oxide nanowires," *Chemical Physics Letters*, vol. 363, no. 1-2, pp. 134–138, 2002.

[14] E. M. Wong and P. C. Searson, "ZnO quantum particle thin films fabricated by electrophoretic deposition," *Applied Physics Letters*, vol. 74, no. 20, pp. 2939–2941, 1999.

[15] V. Srikant and D. R. Clarke, "On the optical band gap of zinc oxide," *Journal of Applied Physics*, vol. 83, no. 10, pp. 5447–5451, 1998.

[16] W. I. Park, G. C. Yi, M. Kim, and S. J. Pennycook, "ZnO nanoneedles grown vertically on Si substrates by non-catalytic vapor-phase epitaxy," *Advanced Materials*, vol. 14, no. 24, pp. 1841–1843, 2002.

[17] X. Q. Meng, D. X. Zhao, J. Y. Zhang et al., "Growth temperature controlled shape variety of ZnO nanowires," *Chemical Physics Letters*, vol. 407, no. 1–3, pp. 91–94, 2005.

[18] H. Tang, J. C. Chang, Y. Shan et al., "Growth mechanism of ZnO nanowires via direct Zn evaporation," *Journal of Materials Science*, vol. 44, no. 2, pp. 563–571, 2009.

[19] G. Shen, Y. Bando, B. Liu, D. Golberg, and C. J. Lee, "Characterization and field-emission properties of vertically aligned ZnO nanonails and nanopencils fabricated by a modified thermal-evaporation process," *Advanced Functional Materials*, vol. 16, no. 3, pp. 410–416, 2006.

[20] D. C. Kim, S. K. Mohanta, and H. K. Cho, "Vertically aligned ultraslim zno nanowires formed by homobuffer: growth evolution and emission properties," *Crystal Growth and Design*, vol. 9, no. 11, pp. 4725–4729, 2009.

[21] F. C. Tsao, J. Y. Chen, C. H. Kuo et al., "Residual strain in ZnO nanowires grown by catalyst-free chemical vapor deposition on GaN/sapphire (0001)," *Applied Physics Letters*, vol. 92, no. 20, Article ID 203110, 3 pages, 2008.

[22] W. Mai, P. Gao, C. Lao et al., "Vertically aligned ZnO nanowire arrays on GaN and SiC substrates," *Chemical Physics Letters*, vol. 460, no. 1–3, pp. 253–256, 2008.

[23] H. Cui, G. Eres, J. Y. Howe et al., "Growth behavior of carbon nanotubes on multilayered metal catalyst film in chemical vapor deposition," *Chemical Physics Letters*, vol. 374, no. 3-4, pp. 222–228, 2003.

[24] H. J. Fan, F. Fleischer, W. Lee et al., "Patterned growth of aligned ZnO nanowire arrays on sapphire and GaN layers," *Superlattices and Microstructures*, vol. 36, no. 1–3, pp. 95–105, 2004.

[25] R. H. Doremus, *In Rates of Phase Transformation*, Academic Press, Orlando, Fla, USA, 1985.

[26] D. A. Porter and K. E. Eastering, *In Phase Transformations In Metals and Alloys*, CRC Press, 2nd edition, 1992.

[27] S. Li, X. Zhang, and L. Zhang, "Sb_2O_3-induced tapered ZnO nanowire arrays: the kinetics of radial growth and morphology control," *Journal of Physical Chemistry C*, vol. 114, no. 23, pp. 10379–10385, 2010.

[28] J. Shi, S. Grutzik, and X. Wang, "Zn cluster drifting effect for the formation of ZnO 3D nanoarchitecture," *ACS Nano*, vol. 3, no. 6, pp. 1594–1602, 2009.

[29] D. H. Kuo and M. Y. Su, "Growth and kinetic modeling of $Fe(CO)_5$-catalyzed carbon nanotubes grown by chemical vapor deposition," *Journal of the Electrochemical Society*, vol. 153, no. 4, pp. J21–J25, 2006.